UC Irvine

UC Irvine Previously Published Works

Title

Precision Measurement of the Ratio B(γ(3S) $\rightarrow$ $\tau^+\tau^-$)/B(γ(3S) $\rightarrow$ $\mu^+\mu^-$)

Permalink

Journal

ISSN

Authors

Lees, JP
Poireau, V
Tisserand, V
et al.

Publication Date

DOI

Copyright Information

Peer reviewed

Precision measurement of the $\mathcal{B}(\Upsilon(3S) \to \tau^+\tau^-)/\mathcal{B}(\Upsilon(3S) \to \mu^+\mu^-)$ ratio

J. P. Lees,[1] V. Poireau,[1] V. Tisserand,[1] E. Grauges,[2] A. Palano,[3] G. Eigen,[4] D. N. Brown,[5] Yu. G. Kolomensky,[5]
M. Fritsch,[6] H. Koch,[6] T. Schroeder,[6] R. Cheaib[b],[7] C. Hearty[ab],[7] T. S. Mattison[b],[7] J. A. McKenna[b],[7] R. Y. So[b],[7]
V. E. Blinov[abc],[8] A. R. Buzykaev[a],[8] V. P. Druzhinin[ab],[8] V. B. Golubev[ab],[8] E. A. Kozyrev[ab],[8] E. A. Kravchenko[ab],[8]
A. P. Onuchin[abc],[8] S. I. Serednyakov[ab],[8] Yu. I. Skovpen[ab],[8] E. P. Solodov[ab],[8] K. Yu. Todyshev[ab],[8] A. J. Lankford,[9]
B. Dey,[10] J. W. Gary,[10] O. Long,[10] A. M. Eisner,[11] W. S. Lockman,[11] W. Panduro Vazquez,[11] D. S. Chao,[12]
C. H. Cheng,[12] B. Echenard,[12] K. T. Flood,[12] D. G. Hitlin,[12] J. Kim,[12] Y. Li,[12] D. X. Lin,[12] T. S. Miyashita,[12]
P. Ongmongkolkul,[12] J. Oyang,[12] F. C. Porter,[12] M. Röhrken,[12] Z. Huard,[13] B. T. Meadows,[13] B. G. Pushpawela,[13]
M. D. Sokoloff,[13] L. Sun,[13, *] J. G. Smith,[14] S. R. Wagner,[14] D. Bernard,[15] M. Verderi,[15] D. Bettoni[a],[16] C. Bozzi[a],[16]
R. Calabrese[ab],[16] G. Cibinetto[ab],[16] E. Fioravanti[ab],[16] I. Garzia[ab],[16] E. Luppi[ab],[16] V. Santoro[a],[16] A. Calcaterra,[17]
R. de Sangro,[17] G. Finocchiaro,[17] S. Martellotti,[17] P. Patteri,[17] I. M. Peruzzi,[17] M. Piccolo,[17] M. Rotondo,[17]
A. Zallo,[17] S. Passaggio,[18] C. Patrignani,[18, †] B. J. Shuve,[19] H. M. Lacker,[20] B. Bhuyan,[21] U. Mallik,[22] C. Chen,[23]
J. Cochran,[23] S. Prell,[23] A. V. Gritsan,[24] N. Arnaud,[25] M. Davier,[25] F. Le Diberder,[25] A. M. Lutz,[25] G. Wormser,[25]
D. J. Lange,[26] D. M. Wright,[26] J. P. Coleman,[27] E. Gabathuler,[27, ‡] D. E. Hutchcroft,[27] D. J. Payne,[27]
C. Touramanis,[27] A. J. Bevan,[28] F. Di Lodovico,[28, §] R. Sacco,[28] G. Cowan,[29] Sw. Banerjee,[30] D. N. Brown,[30]
C. L. Davis,[30] A. G. Denig,[31] W. Gradl,[31] K. Griessinger,[31] A. Hafner,[31] K. R. Schubert,[31] R. J. Barlow,[32, ¶]
G. D. Lafferty,[32] R. Cenci,[33] A. Jawahery,[33] D. A. Roberts,[33] R. Cowan,[34] S. H. Robertson[ab],[35] R. M. Seddon[b],[35]
N. Neri[a],[36] F. Palombo[ab],[36] L. Cremaldi,[37] R. Godang,[37, **] D. J. Summers,[37] P. Taras,[38] G. De Nardo,[39]
C. Sciacca,[39] G. Raven,[40] C. P. Jessop,[41] J. M. LoSecco,[41] K. Honscheid,[42] R. Kass,[42] A. Gaz[a],[43] M. Margoni[ab],[43]
M. Posocco[a],[43] G. Simi[ab],[43] F. Simonetto[ab],[43] R. Stroili[ab],[43] S. Akar,[44] E. Ben-Haim,[44] M. Bomben,[44]
G. R. Bonneaud,[44] G. Calderini,[44] J. Chauveau,[44] G. Marchiori,[44] J. Ocariz,[44] M. Biasini[ab],[45] E. Manoni[a],[45]
A. Rossi[a],[45] G. Batignani[ab],[46] S. Bettarini[ab],[46] M. Carpinelli[ab],[46, ††] G. Casarosa[ab],[46] M. Chrzaszcz[a],[46] F. Forti[ab],[46]
M. A. Giorgi[ab],[46] A. Lusiani[ac],[46] B. Oberhof[ab],[46] E. Paoloni[ab],[46] M. Rama[a],[46] G. Rizzo[ab],[46] J. J. Walsh[a],[46]
L. Zani[ab],[46] A. J. S. Smith,[47] F. Anulli[a],[48] R. Faccini[ab],[48] F. Ferrarotto[a],[48] F. Ferroni[a],[48, ‡‡] A. Pilloni[ab],[48]
G. Piredda[a],[48, ‡] C. Bünger,[49] S. Dittrich,[49] O. Grünberg,[49] M. Heß,[49] T. Leddig,[49] C. Voß,[49] R. Waldi,[49]
T. Adye,[50] F. F. Wilson,[50] S. Emery,[51] G. Vasseur,[51] D. Aston,[52] C. Cartaro,[52] M. R. Convery,[52] J. Dorfan,[52]
W. Dunwoodie,[52] M. Ebert,[52] R. C. Field,[52] B. G. Fulsom,[52] M. T. Graham,[52] C. Hast,[52] W. R. Innes,[52, ‡]
P. Kim,[52] D. W. G. S. Leith,[52, ‡] S. Luitz,[52] D. B. MacFarlane,[52] D. R. Muller,[52] H. Neal,[52] B. N. Ratcliff,[52]
A. Roodman,[52] M. K. Sullivan,[52] J. Va'vra,[52] W. J. Wisniewski,[52] M. V. Purohit,[53] J. R. Wilson,[53]
A. Randle-Conde,[54] S. J. Sekula,[54] H. Ahmed,[55] M. Bellis,[56] P. R. Burchat,[56] E. M. T. Puccio,[56] M. S. Alam,[57]
J. A. Ernst,[57] R. Gorodeisky,[58] N. Guttman,[58] D. R. Peimer,[58] A. Soffer,[58] S. M. Spanier,[59] J. L. Ritchie,[60]
R. F. Schwitters,[60] J. M. Izen,[61] X. C. Lou,[61] F. Bianchi[ab],[62] F. De Mori[ab],[62] A. Filippi[a],[62] D. Gamba[ab],[62]
L. Lanceri,[63] L. Vitale,[63] F. Martinez-Vidal,[64] A. Oyanguren,[64] J. Albert[b],[65] A. Beaulieu[b],[65] F. U. Bernlochner[b],[65]
G. J. King[b],[65] R. Kowalewski[b],[65] T. Lueck[b],[65] I. M. Nugent[b],[65] J. M. Roney[b],[65] A. Sibidanov[b],[65] R. J. Sobie[ab],[65]
N. Tasneem[b],[65] T. J. Gershon,[66] P. F. Harrison,[66] T. E. Latham,[66] R. Prepost,[67] and S. L. Wu[67]

(The BABAR Collaboration)

[1] Laboratoire d'Annecy-le-Vieux de Physique des Particules (LAPP),
Université de Savoie, CNRS/IN2P3, F-74941 Annecy-Le-Vieux, France
[2] Universitat de Barcelona, Facultat de Fisica, Departament ECM, E-08028 Barcelona, Spain
[3] INFN Sezione di Bari and Dipartimento di Fisica, Università di Bari, I-70126 Bari, Italy
[4] University of Bergen, Institute of Physics, N-5007 Bergen, Norway
[5] Lawrence Berkeley National Laboratory and University of California, Berkeley, California 94720, USA
[6] Ruhr Universität Bochum, Institut für Experimentalphysik 1, D-44780 Bochum, Germany
[7] Institute of Particle Physics[a]; University of British Columbia[b], Vancouver, British Columbia, Canada V6T 1Z1
[8] Budker Institute of Nuclear Physics SB RAS, Novosibirsk 630090[a],
Novosibirsk State University, Novosibirsk 630090[b],
Novosibirsk State Technical University, Novosibirsk 630092[c], Russia
[9] University of California at Irvine, Irvine, California 92697, USA
[10] University of California at Riverside, Riverside, California 92521, USA
[11] University of California at Santa Cruz, Institute for Particle Physics, Santa Cruz, California 95064, USA
[12] California Institute of Technology, Pasadena, California 91125, USA

[13]*University of Cincinnati, Cincinnati, Ohio 45221, USA*

[14]*University of Colorado, Boulder, Colorado 80309, USA*

[15]*Laboratoire Leprince-Ringuet, Ecole Polytechnique, CNRS/IN2P3, F-91128 Palaiseau, France*

[16]*INFN Sezione di Ferrara[a]; Dipartimento di Fisica e Scienze della Terra, Università di Ferrara[b], I-44122 Ferrara, Italy*

[17]*INFN Laboratori Nazionali di Frascati, I-00044 Frascati, Italy*

[18]*INFN Sezione di Genova, I-16146 Genova, Italy*

[19]*Harvey Mudd College, Claremont, California 91711, USA*

[20]*Humboldt-Universität zu Berlin, Institut für Physik, D-12489 Berlin, Germany*

[21]*Indian Institute of Technology Guwahati, Guwahati, Assam, 781 039, India*

[22]*University of Iowa, Iowa City, Iowa 52242, USA*

[23]*Iowa State University, Ames, Iowa 50011, USA*

[24]*Johns Hopkins University, Baltimore, Maryland 21218, USA*

[25]*Université Paris-Saclay, CNRS/IN2P3, IJCLab, F-91405 Orsay, France*

[26]*Lawrence Livermore National Laboratory, Livermore, California 94550, USA*

[27]*University of Liverpool, Liverpool L69 7ZE, United Kingdom*

[28]*Queen Mary, University of London, London, E1 4NS, United Kingdom*

[29]*University of London, Royal Holloway and Bedford New College, Egham, Surrey TW20 0EX, United Kingdom*

[30]*University of Louisville, Louisville, Kentucky 40292, USA*

[31]*Johannes Gutenberg-Universität Mainz, Institut für Kernphysik, D-55099 Mainz, Germany*

[32]*University of Manchester, Manchester M13 9PL, United Kingdom*

[33]*University of Maryland, College Park, Maryland 20742, USA*

[34]*Massachusetts Institute of Technology, Laboratory for Nuclear Science, Cambridge, Massachusetts 02139, USA*

[35]*Institute of Particle Physics[a]; McGill University[b], Montréal, Québec, Canada H3A 2T8*

[36]*INFN Sezione di Milano[a]; Dipartimento di Fisica, Università di Milano[b], I-20133 Milano, Italy*

[37]*University of Mississippi, University, Mississippi 38677, USA*

[38]*Université de Montréal, Physique des Particules, Montréal, Québec, Canada H3C 3J7*

[39]*INFN Sezione di Napoli and Dipartimento di Scienze Fisiche,*
Università di Napoli Federico II, I-80126 Napoli, Italy

[40]*NIKHEF, National Institute for Nuclear Physics and High Energy Physics, NL-1009 DB Amsterdam, The Netherlands*

[41]*University of Notre Dame, Notre Dame, Indiana 46556, USA*

[42]*Ohio State University, Columbus, Ohio 43210, USA*

[43]*INFN Sezione di Padova[a]; Dipartimento di Fisica, Università di Padova[b], I-35131 Padova, Italy*

[44]*Laboratoire de Physique Nucléaire et de Hautes Energies, Sorbonne Université,*
Paris Diderot Sorbonne Paris Cité, CNRS/IN2P3, F-75252 Paris, France

[45]*INFN Sezione di Perugia[a]; Dipartimento di Fisica, Università di Perugia[b], I-06123 Perugia, Italy*

[46]*INFN Sezione di Pisa[a]; Dipartimento di Fisica,*
Università di Pisa[b]; Scuola Normale Superiore di Pisa[c], I-56127 Pisa, Italy

[47]*Princeton University, Princeton, New Jersey 08544, USA*

[48]*INFN Sezione di Roma[a]; Dipartimento di Fisica,*
Università di Roma La Sapienza[b], I-00185 Roma, Italy

[49]*Universität Rostock, D-18051 Rostock, Germany*

[50]*Rutherford Appleton Laboratory, Chilton, Didcot, Oxon, OX11 0QX, United Kingdom*

[51]*IRFU, CEA, Université Paris-Saclay, F-91191 Gif-sur-Yvette, France*

[52]*SLAC National Accelerator Laboratory, Stanford, California 94309 USA*

[53]*University of South Carolina, Columbia, South Carolina 29208, USA*

[54]*Southern Methodist University, Dallas, Texas 75275, USA*

[55]*St. Francis Xavier University, Antigonish, Nova Scotia, Canada B2G 2W5*

[56]*Stanford University, Stanford, California 94305, USA*

[57]*State University of New York, Albany, New York 12222, USA*

[58]*Tel Aviv University, School of Physics and Astronomy, Tel Aviv, 69978, Israel*

[59]*University of Tennessee, Knoxville, Tennessee 37996, USA*

[60]*University of Texas at Austin, Austin, Texas 78712, USA*

[61]*University of Texas at Dallas, Richardson, Texas 75083, USA*

[62]*INFN Sezione di Torino[a]; Dipartimento di Fisica, Università di Torino[b], I-10125 Torino, Italy*

[63]*INFN Sezione di Trieste and Dipartimento di Fisica, Università di Trieste, I-34127 Trieste, Italy*

[64]*IFIC, Universitat de Valencia-CSIC, E-46071 Valencia, Spain*

[65]*Institute of Particle Physics[a]; University of Victoria[b], Victoria, British Columbia, Canada V8W 3P6*

[66]*Department of Physics, University of Warwick, Coventry CV4 7AL, United Kingdom*

[67]*University of Wisconsin, Madison, Wisconsin 53706, USA*

We report on a precision measurement of the ratio $\mathcal{R}_{\tau\mu}^{\Upsilon(3S)} = \mathcal{B}(\Upsilon(3S) \to \tau^+\tau^-)/\mathcal{B}(\Upsilon(3S) \to \mu^+\mu^-)$ using data collected with the *BABAR* detector at the SLAC PEP-II e^+e^- collider. The measurement is based on a $28\,\text{fb}^{-1}$ data sample collected at a center-of-mass energy of $10.355\,\text{GeV}$ corresponding to a sample of 122 million $\Upsilon(3S)$ mesons. The ratio is measured to be $\mathcal{R}_{\tau\mu}^{\Upsilon(3S)} =$

2

$0.966 \pm 0.008_{\text{stat}} \pm 0.014_{\text{syst}}$ and is in agreement with the Standard Model prediction of 0.9948 within 2 standard deviations. The uncertainty in $\mathcal{R}_{\tau\mu}^{\Upsilon(3S)}$ is almost an order of magnitude smaller than the only previous measurement.

In the Standard Model (SM) the width of a spin 1 bound state of a quark and antiquark decaying into a charged lepton-antilepton pair in the absence of radiation effects has been known since the model's inception [1] to be:

$$\Gamma_{\ell\ell} = 4\alpha^2 e_q^2 \frac{|\Psi(0)|^2}{M^2} \left(1 + 2\frac{m_\ell^2}{M^2}\right) \sqrt{1 - 4\frac{m_\ell^2}{M^2}},$$

where $\Gamma_{\ell\ell}$ is the decay width to two leptons of flavor ℓ (e.g., muon or τ lepton), α is the fine structure constant, e_q is the quark charge, $\Psi(0)$ is the value of the radial wave function evaluated at the origin, M is the resonance mass, and m_ℓ is the lepton mass. The ratio of widths to final-state leptons with different flavor is free of hadronic uncertainties, and for heavy spin 1 resonances, such as the family of the $b\bar{b}$ bound states $\Upsilon(nS)$ mesons, differs from unity only by a small mass correction. Consequently, leptonic decays of the $\Upsilon(nS)$ mesons are good candidates to test SM predictions and to search for phenomena beyond the SM. For example, the CP-odd Higgs boson A^0 proposed in Ref. [2] couples more strongly to heavier fermions. This would introduce the $\Upsilon(nS) \to \gamma A^0 \to \gamma\tau^+\tau^-$ decay chain with a rate substantially higher than that of the $\Upsilon(nS) \to \gamma A^0 \to \gamma\mu^+\mu^-$ chain and result in a larger value of the ratio $\mathcal{R}_{\tau\mu}^{\Upsilon(3S)} = \mathcal{B}(\Upsilon(3S) \to \tau^+\tau^-)/\mathcal{B}(\Upsilon(3S) \to \mu^+\mu^-)$ than predicted in the SM. The only measurement to date of that ratio was made by the CLEO collaboration, $\mathcal{R}_{\tau\mu}^{\Upsilon(3S)} = 1.05 \pm 0.08 \pm 0.05$ [3]. It has also been remarked [4] that measuring this ratio could shed light on the suggestion for new physics seen in $\Gamma(B \to D^{(*)}\tau\nu)/\Gamma(B \to D^{(*)}(e/\mu)\nu)$ [5]. A new precise measurement will further constrain new physics models.

In this Letter we present a precision measurement of the ratio $\mathcal{R}_{\tau\mu}^{\Upsilon(3S)}$ using a novel technique to discriminate between resonant and non-resonant (i.e., continuum) dimuon production based on differences in the dimuon mass distributions associated with initial state radiation (ISR). In the resonant process, $e^+e^- \to \Upsilon(3S) \to \mu^+\mu^-$, ISR is heavily suppressed compared to the non-resonant, $e^+e^- \to \mu^+\mu^-$, process. Details of how we estimate the non-$\Upsilon(3S)$ contribution to the dimuon sample using this technique are described below. We account for the number of non-resonant $\tau^+\tau^-$ events using information from the continuum values of the number of dimuons together with the ratio of the selected number of $\tau^+\tau^-$ to $\mu^+\mu^-$ events in the $\Upsilon(4S)$ data control sample, corrected for center-of-mass dependent phase-space effects. This method ensures that the measured ratio is fully inclusive of radiation effects and does not require a precise luminosity determination.

The data samples used for these studies were collected with the *BABAR* detector at the PEP-II asymmetric-energy e^+e^- collider at the SLAC National Accelerator Laboratory. The *BABAR* experiment collected data between 1999 and 2008 at center-of-mass energies of the $\Upsilon(4S)$, $\Upsilon(3S)$, and $\Upsilon(2S)$ resonances, as well as at non-resonant energies. The PEP-II positron beam energy was $3.1\,\text{GeV}$, while the electron beam energy was $8.6\,\text{GeV}$ at the $\Upsilon(3S)$ and $9.0\,\text{GeV}$ at the $\Upsilon(4S)$, resulting in different boosts of the final-state system and different detector acceptances in the center-of-mass frame. We measure the ratio $R_{\tau\mu}^{\Upsilon(3S)}$ using a sample of 122 million $\Upsilon(3S)$ decays corresponding to an integrated luminosity of $27.96\,\text{fb}^{-1}$ [6] collected at $\sqrt{s} = 10.355\,\text{GeV}$ during 2008 (referred to as Run 7), where $\sqrt{s}$ is the center-of-mass energy. We also employ three data control samples: data collected at the $\Upsilon(4S)$ in 2007 (referred to as Run 6) corresponding to $78.3\,\text{fb}^{-1}$, data taken $40\,\text{MeV}$ below the $\Upsilon(4S)$ resonance (termed "off-resonance") corresponding to $7.75\,\text{fb}^{-1}$, and data taken $30\,\text{MeV}$ below the $\Upsilon(3S)$ resonance corresponding to $2.62\,\text{fb}^{-1}$. All data used in this analysis were collected with the same detector configuration after the last major upgrade in 2007. These data control samples are used to evaluate properties of the background, to study systematic effects, and to calculate corrections to Monte Carlo (MC) based efficiencies. We employ a blind analysis [7] in which only a small subset of $2.41\,\text{fb}^{-1}$ of the total $\Upsilon(3S)$ sample is used in the pre-unblinding stage during which selection criteria are optimized.

BABAR was a general purpose detector and is described in detail elsewhere [8, 9]. Its magnetic spectrometer, used to measure momenta of charged particles, comprised a 5-layer silicon vertex tracker (SVT) surrounded by a 40-layer cylindrical drift chamber (DCH) placed inside a $1.5\,\text{T}$ superconducting solenoid with its axis aligned nearly parallel to the e^+e^- beams. Charged hadron identification was performed by using ionization measurements in the SVT and DCH and by using a ring-imaging Cherenkov detector (DIRC), which formed a cylinder surrounding the DCH. The *BABAR* electromagnetic calorimeter (EMC), composed of an array of 6580 CsI(Tl) crystals located between the DIRC and the solenoid, was used to measure energies and directions of photons as well as to identify electrons. Muons and neutral hadrons were identified by arrays of resistive plate chambers or limited steamer-tube detectors inserted into gaps in the steel of the Instrumented Flux Return (IFR) of the magnet. An

upgrade of the IFR was completed in 2007 prior to Run 6.

The major irreducible background process is continuum dilepton production. The KKMC event generator [10] is used to simulate continuum $\mu^+\mu^-$ and $\tau^+\tau^-$ production taking into account radiative effects. For the Bhabha process the BHWIDE [11] event generator is employed. The EvtGen generator [12] is used to simulate hadronic continuum events and generic $\Upsilon(3S)$ decays, with the final-state radiation effects modeled by means of the PHOTOS package [13]. The simulated $\mu^+\mu^-$, $\tau^+\tau^-$, and generic $\Upsilon(3S)$ samples correspond to roughly twice the number of events in the $\Upsilon(3S)$ dataset, while the Bhabha sample corresponds to roughly half the number of events. In addition, the $\Upsilon(3S) \to \mu^+\mu^-$ and $\Upsilon(3S) \to \tau^+\tau^-$ signal decays are simulated using the KKMC generator with ISR turned off. Thus the same MC generator, KKMC, is employed for both the signal and continuum, which enables a consistent evaluation of the corrections to the discrepancies between data and MC. This signal MC sample is about three times the size of the data sample. Particle interactions with the detector and its response are modeled within the GEANT4 framework [14].

As mentioned above, the selection criteria are developed using a $2.41\,\mathrm{fb}^{-1}$ $\Upsilon(3S)$ subsample (approximately one-tenth of the total data) to avoid possible biases. The dimuon candidate requires two and only two reconstructed high momentum collinear ($< 20°$) charged particles in the center-of-mass frame with opposite charges and with associated energy depositions in the EMC consistent with the muon hypothesis. We apply a polar angle selection of $37° \lesssim \theta_- \lesssim 143°$ and $33° \lesssim \theta_+ \lesssim 147°$, where θ_- and θ_+ are polar angles in the center-of-mass frame of negative and positive muon candidates respectively. This selection provides the same efficiency at the borders of the sensitive volume for different boost values at different energies in the laboratory frame. Misidentified Bhabha events are additionally suppressed with a requirement that at least one of the muon candidates in an event has a response in the IFR. The scaled invariant mass $M_{\mu\mu}/\sqrt{s}$ of the two muons must be in the range $0.8 < M_{\mu\mu}/\sqrt{s} < 1.1$. These selection criteria provide a dimuon sample with 99.9% purity, according to MC studies.

We consider τ-pairs where both taus have a single charged particle in their decay, where one of the charged particles is an electron and the other is not an electron. The $\tau^+\tau^-$ candidate selection proceeds by requiring two and only two reconstructed tracks with opposite charges in the event. One of the tracks is required to be identified as an electron based on energy deposition in the tracking system and EMC, whereas the other track must fail the same electron selection requirements. Backgrounds are further suppressed by requiring the angle between the two tracks to be greater than 110° in the center-of-mass frame. The total energy registered in the EMC must be less than 70% of the initial e^+e^- energy in the laboratory frame. The acollinearity between the two tracks in the azimuthal plane must be greater than 3°. The missing mass, M_{miss}, which is based on the two tracks and up to the ten most energetic clusters in the EMC identified as photons, must satisfy the requirement that $|M_{\mathrm{miss}}^2/s| > 0.01$. The missing momentum vector must point to the sensitive part of the detector, defined as $|\cos\theta_{\mathrm{miss}}| < 0.85$ in the center-of-mass frame. To further suppress the Bhabha background, the acollinearity angle between the non-electron track and the combination of the identified electron track and the most energetic photon must be greater than 2° in both azimuthal and polar angles in the center-of-mass frame.

A large fraction of the background comes from two-photon processes where tracks have low transverse momenta. Since this region is also populated by the signal $\tau^+\tau^-$ events, a two-dimensional cut on the transverse momentum of the positive lepton *vs* that of the negative lepton is developed to remove the background and maintain an acceptable efficiency for the signal events. These selection criteria provide a $\tau^+\tau^-$ sample with 99% purity, according to MC studies.

The $2.62\,\mathrm{fb}^{-1}$ $\Upsilon(3S)$ off-resonance and $7.75\,\mathrm{fb}^{-1}$ $\Upsilon(4S)$ off-resonance samples are used to correct for differences between MC and data $\tau^+\tau^-/\mu^+\mu^-$ selection efficiency ratios. For the experimental data and their corresponding MC samples, the number of dilepton candidates (MC scaled to the data luminosity) and corresponding efficiency corrections are shown in Table I. For the $\Upsilon(3S)$ and $\Upsilon(4S)$ off-resonance data samples, the $N_{\tau\tau}/N_{\mu\mu}$ dilepton candidate ratios are 0.11665 ± 0.00029 and 0.11647 ± 0.00017, respectively. These are in excellent agreement and show that for these selections the efficiency ratio does not depend on the center-of-mass energy or the different boost associated with the two samples. The corresponding MC samples show the same behavior and allow us to extract data-driven corrections to the MC efficiency ratio. The average correction to the MC efficiency ratio between samples is $C_{\mathrm{MC}} = (\varepsilon_{\tau\tau}/\varepsilon_{\mu\mu})^{\mathrm{data}}/(\varepsilon_{\tau\tau}/\varepsilon_{\mu\mu})^{\mathrm{MC}} = 1.0146 \pm 0.0016$.

TABLE I: The numbers of dilepton candidates in $2.62\,\mathrm{fb}^{-1}$ $\Upsilon(3S)$ and $7.75\,\mathrm{fb}^{-1}$ $\Upsilon(4S)$ off-resonance data and MC samples and the correction for data and MC efficiency discrepancies. The numbers of MC events are scaled according to the measured luminosity.

Sample	$N_{\mu\mu}^{\mathrm{data}}$	$N_{\mu\mu}^{\mathrm{MC}}$	$N_{\tau\tau}^{\mathrm{data}}$	$N_{\tau\tau}^{\mathrm{MC}}$	$\dfrac{N_{\tau\tau}^{\mathrm{data}}/N_{\mu\mu}^{\mathrm{data}}}{N_{\tau\tau}^{\mathrm{MC}}/N_{\mu\mu}^{\mathrm{MC}}}$
$\Upsilon(3S)$	1,538,569	1,554,208	179,466	178,569	1.015 ± 0.003
$\Upsilon(4S)$	4,422,407	4,398,983	515,067	505,133	1.014 ± 0.002

The method to discriminate between $\Upsilon(3S) \to \mu^+\mu^-$ decays and the continuum production $e^+e^- \to \mu^+\mu^-$ is based on the fact that the $\Upsilon(3S)$ resonance is very narrow and thus the ISR effects are highly suppressed for

the signal, but not the continuum background. If the ISR photons have an energy greater than a few MeV (an amount associated with the PEP-II beam energy spread), then the e^+e^- interaction energy is too low to form the $b\bar{b}$ bound state. This effect results in a significant difference in the radiative tail of the $M_{\mu\mu}$ distribution for the continuum and resonance production processes for reconstructed dimuon candidates, as shown in Fig. 1. About 23% of the continuum candidates are in the low mass radiative tail region ($M_{\mu\mu}/\sqrt{s} < 0.98$; 3σ of invariant mass resolution corresponds to approximately 0.02 in these units) whereas for the resonance decays this number is only 7%, and is associated with final state radiation effects.
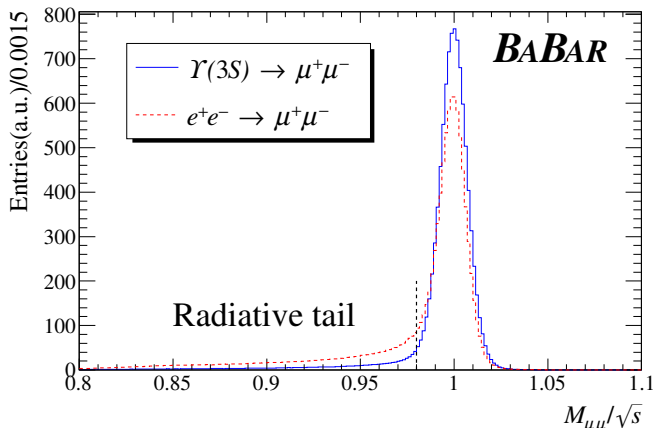
FIG. 1: Comparison of $M_{\mu\mu}/\sqrt{s}$ distributions for the continuum production $e^+e^- \to \mu^+\mu^-$ in data at $\Upsilon(4S)$ off-resonance energy and $\Upsilon(3S) \to \mu^+\mu^-$ decays in MC, where only final-state radiation is expected. The distributions are normalized to the same number of events. The vertical dashed line shows the border $M_{\mu\mu}/\sqrt{s} = 0.98$.

In Fig. 2 the selected signal events are shown for simulated $\Upsilon(3S)$ decays. For the dimuon events, the $M_{\mu\mu}/\sqrt{s}$ variable is plotted whereas for the $\tau^+\tau^-$ events the total reconstructed event energy, scaled to center-of-mass energy, $E_{\tau\tau}/\sqrt{s}$, is plotted. In the dimuon events, decays of the $\Upsilon(3S)$ to lower mass $\Upsilon(1S)$ or $\Upsilon(2S)$ resonances via radiative and hadronic transitions, where the $\Upsilon(1S)$ or $\Upsilon(2S)$ then decay into a dimuon pair, are clearly seen and separated. In this paper we refer to such processes, including analogous processes with a $\tau^+\tau^-$ final state, as "cascade decays". Owing to the excellent momentum resolution of the tracking system, the $M_{\mu\mu}/\sqrt{s}$ distribution provides not only an estimate of the number of $\Upsilon(3S) \to \mu^+\mu^-$ events but also a direct evaluation of the contributions from the cascade decays. In the $\tau^+\tau^-$ channel, however, these cascade decay channels all have the same broad distribution in $E_{\tau\tau}/\sqrt{s}$ and are nearly indistinguishable.

In order to extract the ratio $\mathcal{R}_{\tau\mu}^{\Upsilon(3S)}$ that takes into ac-
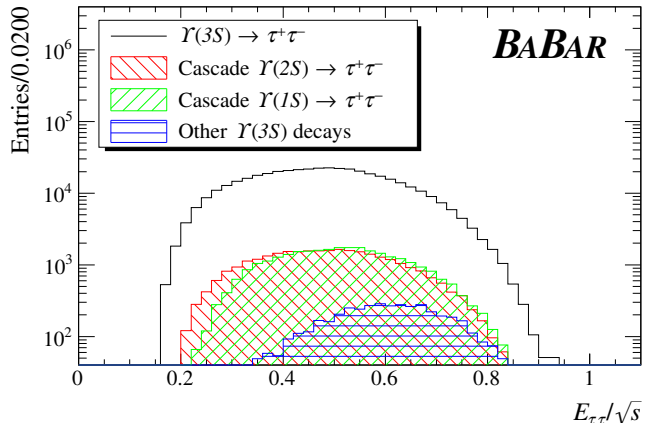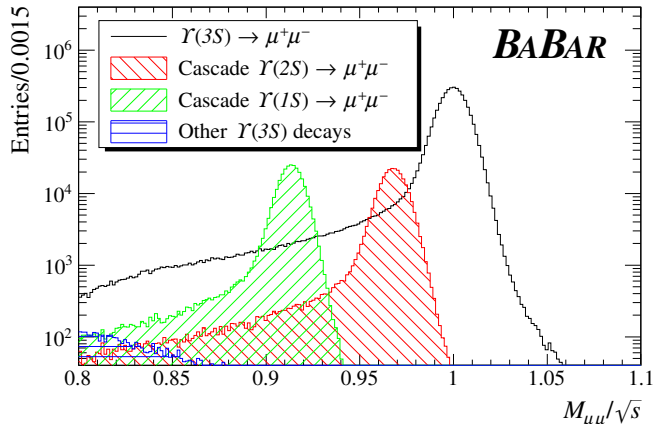
FIG. 2: Distributions of $M_{\mu\mu}/\sqrt{s}$ (top plot) and $E_{\tau\tau}/\sqrt{s}$ (bottom plot) variables in MC. Cascade decays are clearly separated in dimuon events and nearly indistinguishable in $\tau^+\tau^-$ events.

count correlations between components, a binned maximum likelihood fit procedure based on the $M_{\mu\mu}/\sqrt{s}$ and $E_{\tau\tau}/\sqrt{s}$ distributions is employed. The fit procedure is based on the template-fitting method of Ref. [15] and takes into account the finite number of events in the fit-template components. The $\Upsilon(3S) \to \mu^+\mu^-$ and $\Upsilon(3S) \to \tau^+\tau^-$ templates are taken from the KKMC-based MC without ISR effects. The templates for $\Upsilon(2S) \to \ell^+\ell^-$ and $\Upsilon(1S) \to \ell^+\ell^-$ via cascade decays, as well as the remaining small contributions from $\Upsilon(nS)$ hadronic decays, are taken from the EvtGen-based MC. The continuum templates use data control samples, as described in the following paragraph.

The amount of BABAR data collected on-resonance is about ten times larger than off-resonance. Consequently, when the continuum template is based only on the off-resonance data, the small size of that sample dominates the statistical uncertainty of the ratio. To overcome this limitation, $\Upsilon(4S)$ on-resonance Run 6 data, with an integrated luminosity of $78.3\,\mathrm{fb}^{-1}$ and the same detector configuration as Run 7, is used for the continuum template in

the fit. Since the leptonic width of the $\Upsilon(4S)$ is negligible compared to the total width, only continuum-produced dilepton events are expected in the sample. However, other $\Upsilon(nS) \to \ell^+\ell^-$ decays appear in the data continuum template via the ISR process. The radiative return processes have been extensively studied by BABAR (e.g., a narrow resonance production described in Ref. [16]) and based on this approach, the amount of ISR-produced $\Upsilon(nS)$ mesons are estimated and subtracted from the continuum template.

The number of $\Upsilon(3S) \to \mu^+\mu^-$ events $N_{\mu\mu}$ and the raw ratio $\tilde{R}_{\tau\mu} = N_{\tau\tau}/N_{\mu\mu}$ are free parameters of the fit. In the non-signal templates, this ratio is fixed either as in data for the continuum background or to the simulation prediction for the other templates.

A graphical representation of the fit result is shown in Figs. 3 and 4. The fit yields a raw ratio of $\tilde{R}_{\tau\mu} = N_{\tau\tau}/N_{\mu\mu} = 0.10788 \pm 0.00091$. The MC-based selection efficiencies and their ratio, which are needed to obtain the ratio $R_{\tau\mu}$, are shown in Table II.

TABLE II: MC selection efficiencies in percent for $\Upsilon(3S) \to \ell^+\ell^-$. The quoted uncertainties reflect MC statistics.

$\varepsilon_{\mu\mu}$ (%)	$\varepsilon_{\tau\tau}$ (%)	$\varepsilon_{\tau\tau}/\varepsilon_{\mu\mu}$
69.951 ± 0.018	7.723 ± 0.010	0.11041 ± 0.00015

Low multiplicity $\Upsilon(4S) \to B\bar{B}$ decays, such as semileptonic decays, can potentially mimic τ-pair events and then pass the selection criteria. These would modify the $\Upsilon(4S)$-based continuum template. Note that significant numbers of $\Upsilon(4S) \to B\bar{B}$ events are not expected in the final dimuon sample since $M_{\mu\mu}$ of such candidates is too small. To estimate this effect, a MC sample of 265 million $\Upsilon(4S) \to B\bar{B}$ events was processed, which is about three times the size of the $\Upsilon(4S)$ data, and resulted in 15 dimuon and 7644 $\tau^+\tau^-$ candidates. Thus, the $B\bar{B}$ contribution to the muon template can be safely neglected whereas the amount of $\tau^+\tau^-$ candidates translates into a correction of $\delta_{B\bar{B}} = 0.42\%$ to the expected number of $\Upsilon(3S) \to \tau^+\tau^-$ candidates and is applied to the ratio $R_{\tau\mu}$.

Combining the fit result $\tilde{R}_{\tau\mu}$, the ratio of MC efficiencies $\varepsilon_{\mu\mu}/\varepsilon_{\tau\tau}$, the data/MC correction C_{MC}, and the correction from $B\bar{B}$ events $\delta_{B\bar{B}}$, the ratio is

$$\mathcal{R}_{\tau\mu}^{\Upsilon(3S)} = \tilde{R}_{\tau\mu} \frac{1}{C_{\mathrm{MC}}} \frac{\varepsilon_{\mu\mu}}{\varepsilon_{\tau\tau}} \cdot (1 + \delta_{B\bar{B}}) = 0.9662 \pm 0.0084,$$

where uncertainties from the data/MC correction and MC efficiencies are included in the statistical uncertainty.

The sources of the systematic uncertainty in $\mathcal{R}_{\tau\mu}^{\Upsilon(3S)}$ are summarized in Table III.

To assess the particle identification uncertainty, three additional $\tau^+\tau^-$ classifiers were considered. The first used tighter electron selectors for both the τ to electron and the τ to non-electron selection. The second had a
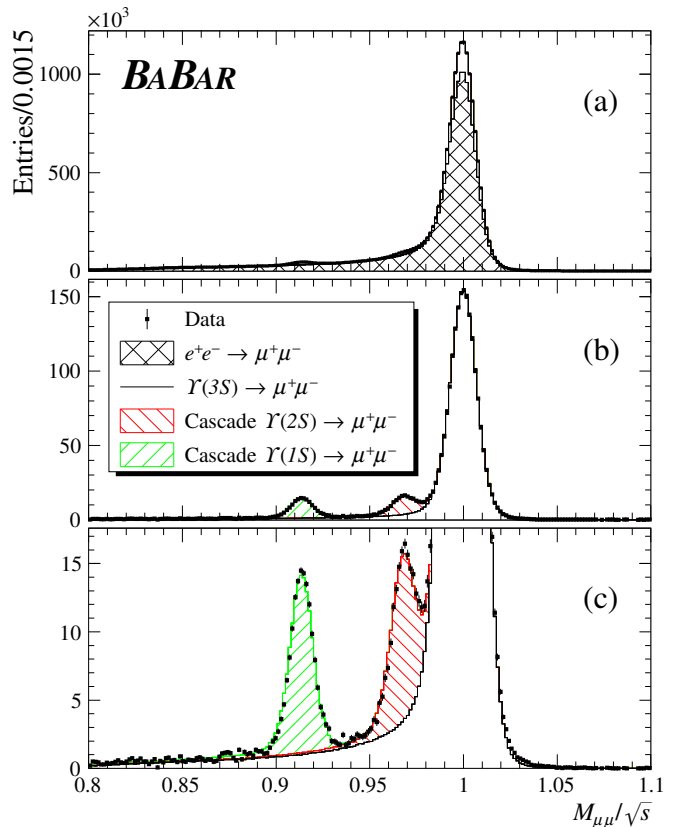

FIG. 3: The result of the template fit to the $\Upsilon(3S)$ data in the $M_{\mu\mu}/\sqrt{s}$ variable. In (a) all events are shown, in (b) and (c) the dominant continuum $e^+e^- \to \mu^+\mu^-$ background is subtracted, and (c) is a magnified view of (b) to better show cascade decays and the radiative tail region.
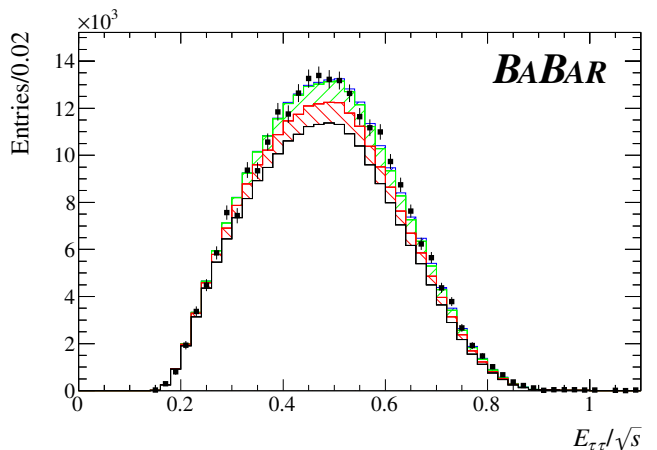

FIG. 4: The result of the template fit to the $\Upsilon(3S)$ data in the $E_{\tau\tau}/\sqrt{s}$ variable after the continuum background is subtracted. Data are depicted as points with error bars. The legend is the same as in the corresponding plot in Fig. 2.

tighter electron selector for the τ to non-electron selection. The third replaced the τ to non-electron selection with an explicit requirement that the non-electron particle be identified as a muon or a pion. Even though the data-driven corrections associated with each of these separate $\tau^+\tau^-$ classifiers were applied, and despite the highly correlated statistics in these samples, there remains a 0.9% difference between one of these three test classifiers and the default classifier, which we assign as the particle identification systematic uncertainty.

The ratio of the number of dimuon and $\tau^+\tau^-$ events from the cascade decays in the MC fit templates are fixed according to lepton-flavor universality. To assess the effect of this assumption, the ratio was varied according to the current experimental uncertainties in branching fractions for $\Upsilon(1S)$ and $\Upsilon(2S)$ to dimuon and $\tau^+\tau^-$ final states, resulting in a maximum difference in $\tilde{R}_{\tau\mu}$ to be 0.6%, which is taken as the systematic uncertainty.

As there is no reliable two-photon fusion MC, the contribution to the systematic uncertainty arising from the two-photon fusion background is estimated by varying the selection on the transverse momentum, which reduces the $\tau^+\tau^-$ selection efficiency to almost half its nominal value. These variations result in a maximal deviation in $\tilde{R}_{\tau\mu}$ of 0.5%.

The simulation of other generic $\Upsilon(3S)$ decays shows that a small fraction of background events (about 0.1% of dimuon and 1% of $\tau^+\tau^-$ samples) still pass the selection criteria. These backgrounds do not exhibit any features that allow them to be easily separated in the fit itself. Because of this, the amount of this background is fixed to the MC prediction and a 0.4% systematic uncertainty is assessed by varying by 50% the background, which is dominated by the $\Upsilon(3S) \rightarrow$hadrons that primarily contaminate the $\tau^+\tau^-$ sample.

To estimate the systematic uncertainty associated with imperfect modeling of radiative effects, the KKMC-based templates for $\Upsilon(3S) \rightarrow \ell^+\ell^-$ decays used in the fit are replaced with templates created using EvtGen with PHOTOS. This primarily modifies the shape associated with radiative tail, shown in Fig. 3, resulting in a change in $\tilde{R}_{\tau\mu}$ of 0.2%. There is a small $\sim 1\%$ difference in $M_{\mu\mu}$ resolution between $\Upsilon(3S)$ and $\Upsilon(4S)$ data, as well as the same order of magnitude difference between data and MC. To estimate the systematic uncertainty due to this difference, the mass resolution in the MC is degraded to be up to 10% worse than the resolution in data. This results in a shift in $\tilde{R}_{\tau\mu}$ of up to 0.4%. From this study, the uncertainty from the MC template shape mismodeling of $\Upsilon(3S) \rightarrow \mu^+\mu^-$ is conservatively estimated to be 0.4%. The total systematic uncertainty from the MC shape modelling associated with the radiative and resolution effects is 0.4%.

The uncertainty from the $B\bar{B}$ background in the continuum template is estimated by varying the expected amount of the background by 50%, resulting in a 0.2% change in the ratio.

The systematic uncertainty associated with $\Upsilon(nS)$ mesons produced by the radiative return process in the continuum template is estimated by accounting for experimental uncertainties of total widths and leptonic branching fractions of these mesons and by varying the overall amount of these produced mesons by 10% in order to conservatively account for radiator function uncertainties. We assign a value of 0.2% as the systematic uncertainty coming from these various effects.

All of the systematic uncertainties described in the paragraphs above are combined in quadrature, giving total systematic uncertainty of 1.4%.

In conclusion, based on the data collected by the *BABAR* detector near the $\Upsilon(3S)$ and $\Upsilon(4S)$ resonances, the ratio of the leptonic branching fractions of the $\Upsilon(3S)$ meson is measured to be

$$\mathcal{R}_{\tau\mu}^{\Upsilon(3S)} = 0.966 \pm 0.008_{\text{stat}} \pm 0.014_{\text{syst}}.$$

This is in agreement with the SM prediction of 0.9948 [4] within two standard deviations and its uncertainty almost an order of magnitude smaller than the only previous measurement reported by the CLEO collaboration [3].

TABLE III: The summary of systematic uncertainties.

Source	Uncertainty (%)
Particle identification	0.9
Cascade decays	0.6
Two-photon production	0.5
$\Upsilon(3S) \rightarrow$ hadrons	0.4
MC shape	0.4
$B\bar{B}$ contribution	0.2
ISR subtraction	0.2
Total	1.4

* Now at: Wuhan University, Wuhan 430072, China
† Now at: Università di Bologna and INFN Sezione di Bologna, I-47921 Rimini, Italy

‡ Deceased

§ Now at: King's College, London, WC2R 2LS, UK

¶ Now at: University of Huddersfield, Huddersfield HD1 3DH, UK

** Now at: University of South Alabama, Mobile, Alabama 36688, USA

†† Also at: Università di Sassari, I-07100 Sassari, Italy

‡‡ Also at: Gran Sasso Science Institute, I-67100 LAquila, Italy

[1] R. Van Royen and V. F. Weisskopf, Nuovo Cim. A **50**, 617 (1967); Erratum: Nuovo Cim. A **51**, 583 (1967).

[2] M. A. Sanchis-Lozano, Int. J. Mod. Phys. A **19**, 2183 (2004).

[3] D. Besson *et al.* (CLEO Collaboration), Phys. Rev. Lett. **98**, 052002 (2007).

[4] D. Aloni, A. Efrati, Y. Grossman and Y. Nir, J. High Energ. Phys. **06**, 019 (2017).

[5] Y. Amhis *et al.* (HFLAV Group), Eur. Phys. Jour. C **77**, no.12, 895 (2017).

[6] J.P. Lees *et al.* (*BABAR* Collaboration), Nucl. Instrum. Methods Phys. Res., Sect. A **726**, 203 (2013).

[7] J. R. Klein and A. Roodman, Ann. Rev. Nucl. Part. Sci. **55**, 141 (2005).

[8] B. Aubert *et al.* (*BABAR* Collaboration), Nucl. Instrum. Methods Phys. Res., Sect. A **479**, 1 (2002).

[9] B. Aubert *et al.* (*BABAR* Collaboration), Nucl. Instrum. Methods Phys. Res., Sect. A **729**, 615 (2013).

[10] B. F. L. Ward, S. Jadach and Z. Was, Nucl. Phys. Proc. Suppl. **116**, 73 (2003).

[11] S. Jadach, W. Placzek, B. F. L. Ward, Phys. Lett. B **390**, 298 (1997).

[12] D. J. Lange, Nucl. Instrum. Methods Phys. Res., Sect. A **462**, 152 (2001).

[13] E. Barberio and Z. Was, Comput. Phys. Commun. **79**, 291 (1994).

[14] S. Agostinelli *et al.* (GEANT4 Collaboration), Nucl. Instrum. Methods Phys. Res., Sect. A **506**, 250 (2003).

[15] R. J. Barlow and C. Beeston, Comput. Phys. Commun. **77**, 219 (1993).

[16] B. Aubert *et al.* (*BABAR* Collaboration), Phys. Rev. D **69**, 011103 (2004).